HYSTERESIS MODELLING FOR A *MR* DAMPER

Jorge de-J. Lozoya-Santos[1], Sebastien Aubouet[2], Ruben Morales-Menendez[1], Olivier Sename[2], Ricardo A. Ramirez-Mendoza[3], Luc Dugard[2]

[1]Tecnologico de Monterrey, Campus Monterrey,
64849 Monterrey, NL, Mexico
[2]GIPSA-Lab, Control Systems Department, CNRS-Grenoble INP ENSE[3], BP 46,
F-38402 St Martin d'Hères cedex, France
[3]Tecnologico de Monterrey, Campus Ciudad de Mexico,
14380 DF, Mexico

rmm@itesm.mx(Ruben Morales-Menendez)

Abstract

An experimental dataset of a commercial Magneto-Rheological (MR) damper is exploited for identification of a Hysteresis-based Control-Oriented model. The model wellness for hysteresis, saturation and transient responses is shown through validation with experimental data. A study case that includes a *Quarter of Vehicle (QoV)* shows that the hysteresis phenomena could affect the primary ride and vehicle handling. Several analysis based on open and closed loop simulation demonstrated that hysteresis must be considered for controller design.

Keywords: hysteresis, MR damper model, model simulation, vehicle dynamics

Presenting Author's Biography

Ruben Morales-Menendez holds a PhD Degree in Artificial Intelligence from Tecnologico de Monterrey. From 2000 to 2003, he was a visiting scholar with the Laboratory of Computational Intelligence at the University of British Columbia, Canada. For more than 23 years, he has been a consultant specializing in the analysis and design of automatic control systems for continuous processes. He is a member of the National Researchers System of Mexico (Level I) and a member of IFAC TC 9.3.

1 Introduction

The Magneto-Rheological (*MR*) damper is a non-linear component with dissipative capability used in the control of semi-active suspensions, where the damping coefficient varies according to the applied electric current. The modelling of the force-velocity curve is not a trivial task due to the hysteresis loop and nonlinear behavior. The *MR* damper inherits the hysteresis and bilinear behavior from its MonoTube (*MT*) mechanical design. Several *MT* damper modelling approaches show that the acceleration $\ddot{z}_{def}$ and velocity $\dot{z}_{def}$ as input variables are needed for a precise hysteresis simulation, [1, 2], and for a realistic simulation of chassis acceleration, suspension deflection and road holding, [3, 4]. A *MR* damper model including the hysteresis becomes necessary in order to obtain precise simulations.

This paper presents a *MR* damper model based on the arrangement of two devices that models the passive force consisting of a spring and a damper, and a damper which models the force due to the current effect over the oil viscosity. The model captures the hysteresis and the current effect achieving frequency independent parameters. The study of the hysteresis compliance is done through a comparison of two modelling approaches in the suspension of a *Quarter of Vehicle (QoV)*.

This document is organized as follows. A theoretical background on *MR* damper modelling and its challenging issues are exposed in section 2. Section 3 presents the proposed model, and experimentation and identification procedure. A study case is presented in Section 4. Section 5 discusses the findings and results. The conclusion is presented in section 6. Table 1 defines the paper nomenclature.

2 Theoretical background

Some fundamental concepts are reviewed, [5]:

(a) When a certain magnetic field is applied to the *MR* fluids, the particles in the fluids are polarized and they form polarization chains, in the parallel direction to the applied field.

(b) When the MR fluids are subjected to an external shear stress in the perpendicular direction to the magnetic field, those polarization chains can resist the shear stress to some extent, and the *MR* fluids behave in a viscoelastic way. This region is referred to as the pre-yield region. When the external shear stress is increased and exceeds a certain value, the polarization chains will be broken and *MR* fluids becomes in regular Newtonian fluids; this region is referred to as the post-yield region.

(c) The gradually decreasing shear stress links up the polarization chains, but the stress value to do the link is less than before the polarization chains break happens, producing the *hysteresis*. The switch of *MR* fluids from viscoelastic behavior to regular Newtonian fluid behavior is referred to as *yield*, and the value of the external shear stress at this point is thus known as *yield stress*, and depends on the intensity of the applied field. Since the polarization chains are increased with the magnetic

Tab. 1 Nomenclature

a_i	Coefficient depending polynomially on the current
c_{MR}	*MR* damping coefficient in $(N \cdot A)/m$
c_p	Passive damping coefficient in Ns/m
h_h	Coefficients dealt with the horizontal hysteresis
k_p	Passive stiffness coefficient in N/m
f_{MR}	*MR* damping observed force in N
f_p	Force due to damper mechanics (N)
f_I	Force due to MR fluid (N) and I
$\hat{f}_{MR}$	Predicted force
h	Input magnetization rate into a ferromagnetic material
c_2, c_3	Magnetic saturation due to remanent magnetism and minor loops
f_+	Positive magnetic saturation level for positive h
f_-	Negative magnetic saturation level for negative h
h_i	Coefficient for the minor loops and dc bias
h_{s1}, h_{s2}, h_{s3}	Coefficients for the hysteresis
h_v	Coefficient for vertical hysteresis
I	Applied current in A
q	Exponent for I in the polynomial
r	Polynomial order for the polynomial current dependency
t	Time
y_1, y_2	Coefficients for the *MR* sigmoid behavior
x, z, z_{def}	Piston deflection in meters
$\dot{x}, \dot{z}, \dot{z}_{def}$	Piston deflection velocity in m/s
$\ddot{x}, \ddot{z}$	Piston deflection acceleration in m/s^2
$\dot{z}_s$	Chassis velocity in m/s
$\ddot{z}_s$	Chassis acceleration in m/s^2
w	Disturbation shaped as chirp sinusoidal
$\alpha_{q,i}$	i-th coefficient for the polynomial current equation
θ	Parameters vector
$\phi_{dataset}$	the input dataset matrix
i	ith input dataset row
$Z_{def}, \dot{Z}_{def}, \ddot{Z}_{def}, I$	Column vectors of the experimental dataset experimental dataset
ω	Frequency in rad/s
f_{XX-MR}	*MR* damping force estimation. The letters XX can be *CO* or *HCO*
$f_{steering}$	Force generated for a steering action
$f : a \mapsto b$	The function f maps the element a to the element b
R	Sinusoidal amplitude in m

field, the shear stress need to be large in order to break them. The larger the magnetic field, the larger the yield force.

A *MR* damper is usually characterized by the displacement and/or velocity of the piston, the electric current applied to the coil as inputs and the force generated on the piston as output. A static *MR* damper model is build having direct or instantaneous links between input variables, thus it esimates the force using the present current and displacement/velocity and not earlier values. A *dynamic MR* damper model is also built with the same variables but these variables change before affecting the force value by their intrinsic dynamics, and their values will thereby also depend on early current or displacements.

A classification for this device is proposed by its original structure as: passive and I-driven. A passive original model does not include the electric current as input variable while the I-driven model does. In the literature, the *MR* damper modelling has been based in all the known model structures: phenomenological (parameters which meaning is related to the mechanical parts, physical meaning), semi-phenomenological (parameters with physical meaning) and the black-box support.

2.1 Passive models

The *MR* damper is often described by the general form:

$$f_p = [\ g(\dot{x}, x) \mid \theta\ ]$$

where the fluid is *MR*. Therefore, the study of the static curves force-velocity and the transient response have been the basis of such models. The consequence is the missing of the electric current (or voltage) as a model input, Fig. 1.

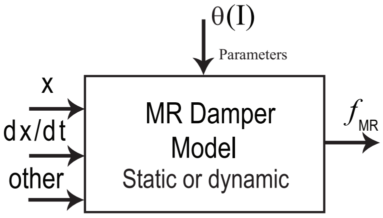

Fig. 1 Passive *MR* damper model

The electric current effect on the damping force is addressed by the representation of each model parameter as a polynomial function of the current; hence, the model is represented as

$$f_{MR} = [\ g(\dot{x}, x) \mid \theta(I)\ ] \quad a_i(I) = \sum_{q=0}^{r} \alpha_{q,i} \cdot I^q \quad (1)$$

Consequently, there is an over-parameterization, and if the polynomial order is greater than 1, the nonlinear complexity is augmented. The main properties of the model are not improved. There are several important works: Bingham model [6], Bouc Wen Modified [7], Polynomial Approach [8], Three Parameters model [9], Sigmoidal-based Behavior model [10], and Phase-Transition model [5]. Table 2 compares some works in this field.

Tab. 2 Classification of the literature passive models. Application capability of the model: d for diagnostic, e for estimation and c for controller synthesis. Hysteresis means the model capability in order to capture the hysteresis. θ length is the model number quantity. $\theta(I)$ length defines the possible number of parameters when the model must be polynomially dependent on the current.

Features	Bouc Wen Modified	Polynomial	Semi-physical	Phase transition
Application	e	e	d	d
θ length	7	12	5	5
Hysteresis	Yes	Yes	No	No
I as input	No	Yes	No	No
$\theta(I)$ length	14	-	30	30
Type	Dyn	Static	Static	Dyn
Frequency dependent parameters	Yes	No	Yes	Yes
Inputs	$f(z, \dot{z})$	$f(\dot{z})$	$f(z, \dot{z})$	$f(\dot{z})$
Fitting method	NLSM	LSM	LSM	NLSM

2.2 I-driven models

The *MR* damper is described by

$$f_{MR} = [\ g(\dot{x}, x, I) \mid \theta\ ]$$

This model considers the applied current as a model input variable, Fig. 2.

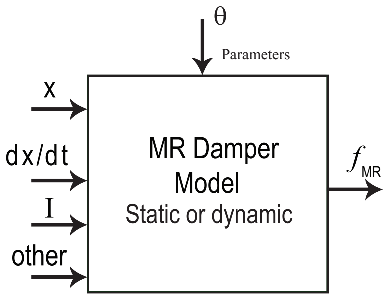

Fig. 2 I-driven *MR* damper model

The parameter identification requires of experiments obtained with persistent excitation in both displacement and current. The modelling contributions are classified as Surface Response Method or Statistical model [11], the Nonlinear Auto-Regressive with eXogenous input (*NARX*) model [12], *NARX* based in Neural Networks (*NNARX*) [13], considered as black box or non-parametric models, and the Dynamic Transfer function Current-Force [14], which analyzes the transient behavior of the force due to the electric current. Table 3 compares some features of those approaches.

Tab. 3 Classification of the literature I-driven models. Same nomenclature as in Table 2.

Features	NARX	NNARX	Statistical
Application	e	e	d
θ length	12	-	5
Hysteresis	Yes	Yes	No
I as input	Yes	Yes	Yes
Type	Dyn	Dyn	Static
Frequency dependent parameters	No	No	No
Inputs	$f(I, z, \dot{z})$	$f(I, z, \dot{z})$	$f(I, z, \dot{z})$
Fitting method	LSM	Levenberg-Marquardt	Surface Response

Tables 2 and 3 compare the main features and characteristics of *MR* damper models. Based on this comparison, some demands are found: (a) the hysteresis phenomena has not been addressed with success given that the analytical models are based on static force-velocity curves where the applied electric current is constant and they lack of the acceleration $\ddot{z}$ as input, an important inertial element in the damping force [1], (b) If the experimental database has static currents, the current could be defined as a varying parameter, where the continuous-time variation of this parameter is considered, (c) there is a necessity for a control-oriented model given that the literature models are proper for estimation or diagnosis and their application for controller synthesis becomes involved.

3 *MR* damper modelling

A general *MR* damper structure model can be described by two dampers in parallel: a damper with constant shear stress (passive) and a damper with variable-shear stress (semi-active) due to the variation of the applied electric current. The sum of these components yields the *MR* total damping force f_{MR}.

$$\begin{aligned} f_{MR} &= f_p(z, \dot{z}) + f_I(z, \dot{z}, I) \\ f_p &= k_p z + c_p \dot{z} + o(z, \dot{z}, \ddot{z}) \\ f_I &= c_{MR} \cdot I \cdot g(\dot{z}, z) \end{aligned} \tag{2}$$

where $o(\cdot)$ and $g(\cdot)$ are nonlinear functions. $o(\cdot)$ describes hysteresis and $g(\cdot)$ describes the semi-active behavior.

3.1 Hysteresis-based Control-Oriented (*HCO*) Model

Equation (3) can represent a magnetic saturation curve with sigmoid T-shape T for a h, [15].

$$T(h) = A_0 \cdot h + B_0 \cdot tanh\left[C_0 \cdot h\right] \tag{3}$$

In order to develop the mathematical expression for a hysteresis loop, the translation of the $T(h)$ function horizontally is done by $\pm a_0$ as vertically by $\pm b_1$. The sign $\pm$ specifies directions,

$$T(h) = A_0 \cdot h + B_0 \cdot tanh\left[C_0 \cdot h - a_0\right] + b_1 + c_2 \tag{4}$$
$$T(h) = A_0 \cdot h + B_0 \cdot tanh\left[C_0 \cdot h + a_0\right] - b_1 + c_3 \tag{5}$$

where the measure of the horizontal shift a_0 represents the value of the coercive force, where the hysteresis loop intersects the horizontal axis. The value of b_1 is determined by h_{max}, the maximum value of h where the two curves f_+ and f_- intersect. The values of c_2 and c_3 represent the minor loops and the remanent magnetism. The *minor loops*, is a collective name of all the loops, which have at least one extreme different from the *major loop* extreme. When the exciting magnetic field is interrupted during the process of magnetization, then the magnetization of the sample will not stay the same, it declines to a value below the value determined by the field at the point of the interruption on the hysteresis loop, phenomenon called *remanent magnetism*.

The Force-Velocity (*FV*) damper map is a well known diagram with high complexity. It exposes the damping ratio ζ behavior. If ζ has a one-to-one relation, the next sentence is true, based on (3).

Let $\zeta : \dot{z} \mapsto h, \; f_{MR} \mapsto T(h)$ be defined by $\zeta(\dot{z}, f_{MR}) = f_{MR}/\dot{z}$.

represents the damper behavior without hysteresis and constant current. In order to obtain a more precise mathematical approach of a damper, the following assumptions and analogies are proposed.

By assuming a harmonic motion of the damper piston, let $z, \dot{z}, \ddot{z}$ approximated by:

$$z \sim R \cdot sin(\omega \cdot t) \tag{6}$$
$$\dot{z} \sim \omega \cdot R \cdot cos(\omega \cdot t) \tag{7}$$
$$\ddot{z} \sim -(\omega)^2 \cdot R \cdot sin(\omega \cdot t) \tag{8}$$

It has been shown that the acceleration deflection $\ddot{z}$ is the stronger influence on shaping of the hysteresis, [1, 2]. The $\ddot{z}_{def}$ inertial effect contributes to the hysteresis offset. From equations (4, 5), and based on [1, 2, 10, 16], the static mapping defined in [15] is extended to a dynamic mapping

$$H_h : h_h \cdot z \mapsto a_{0dynamic} \tag{9}$$
$$H_i : h_i \cdot z \mapsto c_{1,3dynamic} \tag{10}$$
$$H_v : h_v \cdot \ddot{z} \mapsto b_{1dynamic} \tag{11}$$

Thus, the values for the coefficients defined in (4) and (5) will change according to z, $\dot{z}$ and $\ddot{z}$. The hysteresis loop will be shaped depending on the piston motion dynamics. The proposed model is defined by:

$$\begin{aligned} f_{MR} = \; & k_p z + c_p \dot{z} + h_v \cdot \ddot{z} + \\ & h_{s2} \cdot tanh\left(h_{s3} \cdot \dot{z} + h_h \cdot z\right) + \\ & c_{MR} \cdot I \cdot tanh\left(y_1 \cdot \dot{z} + y_2 \cdot z\right) \end{aligned} \tag{12}$$

where $c_p = h_{s1}$ and $k_p = h_i$, and the sigmoid function defines the shape accuracy. This model is an I-driven full model because it includes the current, the deflection and its first and second derivatives of the deflection as inputs.

3.2 Control-Oriented (*CO*) model structure

. Modifying the Semi-Phenomenological model [10], an I-driven model (13) can be proposed. This modelling approach performs good simulations of the bi-viscous and saturation behavior but limits the hysteresis representation.

$$f_{MR} = c_{MR} \cdot I \cdot tanh\left(y_1 \cdot \dot{z} + y_2 \cdot z\right) + c_p \cdot \dot{z} + k_p \cdot z \quad (13)$$

3.3 Experimental data and identification

A *Frequency modulated* displacement with *ICPS* electric current as input signal was exploited in order to identify the *MR* damper in a experimental system, [16]. The models represented by equations (12,13) are identified by using the nonlinear least square curve fit algorithm with the following cost function:

$$\min_{\theta} ||\hat{f}_{MR}(\theta, \phi_{dataset}) - f_{MR}||_2^2 = \min_{\theta} \sum_i \left(\hat{f}_{MR}(\theta, \phi_i) - f_{MRi}\right)$$

where $\phi_{dataset} = [Z_{def}, \dot{Z}_{def}, \ddot{Z}_{def}, I]$.

4 Study case

The system consists of a simple model of a Quarter of Vehicle (*QoV*). The main components are the sprung mass (m_s) and the unsprung mass (m_{us}). The spring with a stiffness coefficient k_s and a semi-active damper built the suspension between masses. The stiffness coefficient k_t models the wheel tire. The vertical position of the mass m_s (m_{us}) is defined by z_s (z_{us}). It is assumed that the wheel contact is kept.

The used *QoV* parameters corresponds to a *Renault Megane Coupe*^{TM} model (see [17]) whose values are: m_s = 315 Kg, m_{us} = 37.5 Kg, k_s = 29500 N/m, k_t = 210000 N/m. The damper parameters are defined according to equations. (13) and (12).

Two *QoV* simulation systems with a semiactive suspension were implemented. They used *MR* damper models (12) and (13) resulting equations (15) and (17), called *linear QoV* and *nonlinear QoV* respectively. The steering force is considered zero. The *linear* word is used in the sense of the hysteresis phenomena presence on the *MR* damper.

The dynamical equations for the *linear QoV* are governed by:

$$\begin{aligned} m_s \ddot{z}_s &= -k_s \cdot z - f_{CO-MR} + f_{steering} \\ m_{us} \ddot{z}_{us} &= k_s \cdot z + f_{CO-MR} - k_t\left(z_{us} - z_r\right) \end{aligned} \quad (14)$$

where the f_{CO-MR} is estimated by:

$$\begin{aligned} f_{CO-MR} \approx\ & c_p \cdot \dot{z} + k_p \cdot z \\ & + c_{MR} \cdot I \cdot tanh\left(y_1 \cdot \dot{z} + y_2 \cdot z\right) \end{aligned} \quad (15)$$

and it uses the parameters for the *CO MR* damper model shown in Table 4.

The dynamical equations for the *nonlinear QoV* are governed by:

$$\begin{aligned} m_s \ddot{z}_s &= -k_s \cdot z - f_{HCO-MR} + f_{steering} \\ m_{us} \ddot{z}_{us} &= k_s \cdot z + f_{HCO-MR} - k_t\left(z_{us} - z_r\right) \end{aligned} \quad (16)$$

where the f_{HCO-MR} is estimated by:

$$\begin{aligned} f_{HCO-MR} \approx\ & k_p z + c_p \dot{z} + h_v \cdot \ddot{z} + \\ & h_{s2} \cdot tanh\left(h_{s3} \cdot \dot{z} + h_h \cdot z\right) + \\ & c_{MR} \cdot I \cdot tanh\left(y_1 \cdot \dot{z} + y_2 \cdot z\right) \end{aligned} \quad (17)$$

and it uses the parameters for the *HCO MR* damper model shown in Table 4.

It is worth to note that when the applied current equals 0 A, the passive damping is approached by a linear coefficient in equation (15). The frequency response or pseudo-bode, [18]), of both systems exposes the controllability margins with and without hysteresis inclusion.

Two simulation tests were done: open and closed control systems, Figure 3.

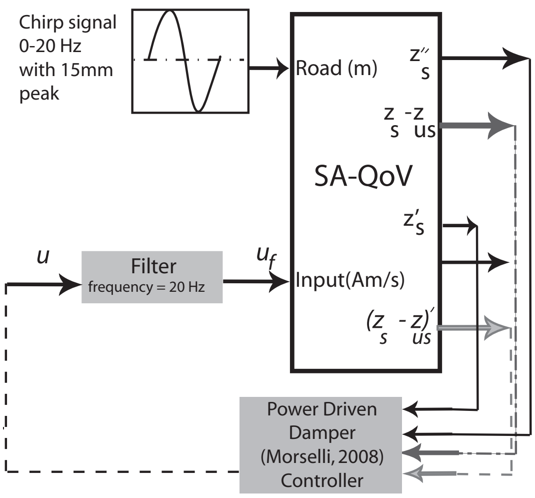

Fig. 3 Diagram of simulation for the quarter of vehicle in open and closed loop. The controller input signals are considered measurable. The filter block is required in order to assure soft changes when the control law switches between the commanded current values, defined in (18). The filter cut-off frequency must be at least 20 hz in order to cover the automotive bandwidth.

The applied current was {0.001,0.5,1,1.5,2,2.5} A for the open control system. For the closed control system, comfort oriented controller *Power-Driven-Damper Control (*PDD*)*, [19], evaluates both systems. The specifications for the comfort, [20], are defined in the span of [0-10] Hz, the maximum gain of the frequency response $\ddot{z}_s/z_r$ must be kept low below 200. The (*PDD*) control strategy is obtained from control of Hamiltonian port systems and claims for soft manipulations and good performance under ω = 120 rad/s.

The closed control input input is the current, hence, the control strategy has been modified in order to be proper for the *MR QoV* suspension. The modified *PDD* control law is:

$$
\begin{array}{l}
I_{min} \\
\quad \text{if } \; K \cdot z_{def} \cdot \dot{z}_{def} + b_{max}\dot{z}_{def}^2 < 0 \\
I_{max} \\
\quad \text{if } \; K \cdot z_{def} \cdot \dot{z}_{def} + b_{min}\dot{z}_{def}^2 \geq 0 \\
(I_{max} + I_{min})/2 \\
\qquad \text{if } \; \dot{z}_{def} = 0 \quad and \quad z_{def} \neq 0 \\
I_{max} \cdot z_{def}/\dot{z}_{def} \quad \text{otherwise}
\end{array}
\tag{18}
$$

where $K = k + k_p$, b_{max} corresponds to the MR damper model force evaluated in $\dot{z}_{def}$ at maximum current 2.5 A and divided between $\dot{z}_{def}$ m/s, b_{min} corresponds to the MR damper model force evaluated in $\dot{z}_{def}$ at cero current and divided between $\dot{z}_{def}$ m/s. The values for I_{min} and I_{max} where defined as 0.2 and 2.5 A. See Figure 3 for the simulation diagram and filter frequencies for the controller.

5 Discussion

Table 4 shows the identified parameters.

Tab. 4 Identified parameters from the experiment

Model	c_{MR}	c_p	k_p	y_1	y_2
CO	441	636	-20356	12	14.3
HCO	444	246	5977	7.12	7.9
Model	h_h	h_{s2}	h_{s3}	h_v	-
HCO	-37.6	-141	-46	-13.8	-

The descriptive force-velocity curves shows the good tracking of the hysteresis with the model *HCO*, left top plot in Fig. 4. The model *CO* makes good saturation estimation but at low velocity the precision is small, right top plot in Fig. 4. The force-velocity curves, bottom plot in Fig. 4, exposes the covering done by each model versus real data where the real hysteresis matches in a more precise shape for model *HCO*.

In transient response, the model *HCO* becomes more accurate for small and big forces. The model *CO* fails the estimation for small forces ($\leq$ 200 N) because the inertial effects are missing the model. See the models error at low forces on Fig. 5.

The classification of the evaluated models shows better features than the aforementioned reviewed, Table 5, adding an easier process for their identification. A wide analysis is necessary in order to define the frequency dependence of the parameters.

The open loop tests exposes a different controllability when the suspension includes hysteresis and when it does not, see Fig. 6. In the span of primary ride (0-2.5 Hz) the nonlinear case shows a more realistic and constrained controllability than its linear counterpart. For maximum current and rattle-space frequency (the chassis and the tire fixture can shock each other, approx.

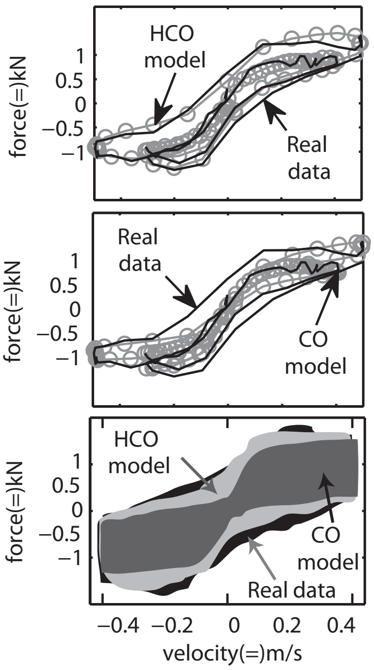

Fig. 4 Attitude of *MR* damper models in force-velocity curves: detailed and general views.

Tab. 5 Classification of the proposed models. The categories are the same as for table 2.

Features	CO model	HCO model
Application	d,e,c	d,e,c
θ length	5	9
Hysteresis	No	Yes
Type	Static	Static
Inputs	$f(I, z, \dot{z})$	$f(I, z, \dot{z}, \ddot{z})$
Fitting method	LSM	LSM

1.8 Hz), referring to the linear case, the $\ddot{z}_{def}$ shows very low gain and very good comfort while the nonlinear case is more conservative. In the spans of (2.5-11 Hz) and (16-20 Hz) both approaches offer similar performances, but the minimum gain is greater with hysteresis. In (11-16 Hz), the simulation results show how the tire-hop (the tire can be separated from the surface) frequency is affected by the hysteresis being an interesting and important result in the evaluation on controllers, given that this frequency is key for the vehicle handling. The simulation allows to infere that in this bandwidth, high currents are desired in order to improve the vehicle stability.

The closed loop test offers more illustrative results. The controller is very efficient when the semi-active suspension does not include the hysteresis (similar to that reported in [19]). When the hysteresis is taken into account, i. e. the *MR* damper is *HCO* model, the controller performs as expected for 2-8 Hz but for the rattle-space frequency the performance is very poor from the obtained without hysteresis.

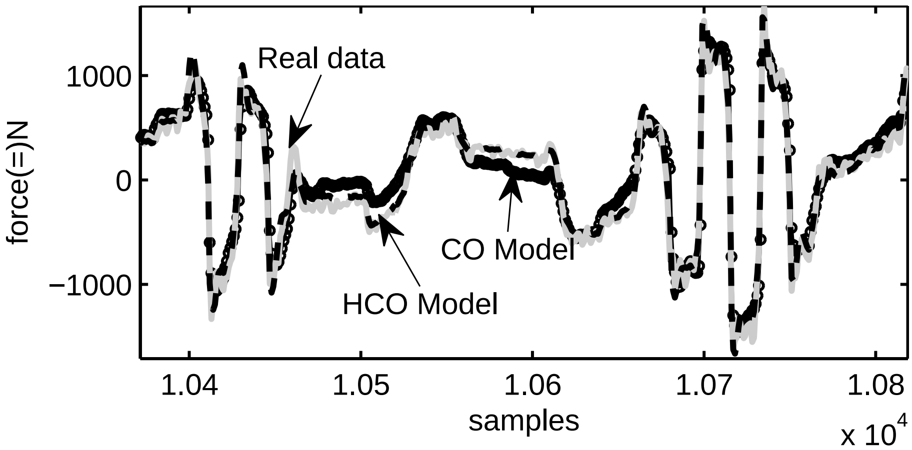

Fig. 5 *MR* damper models transient response

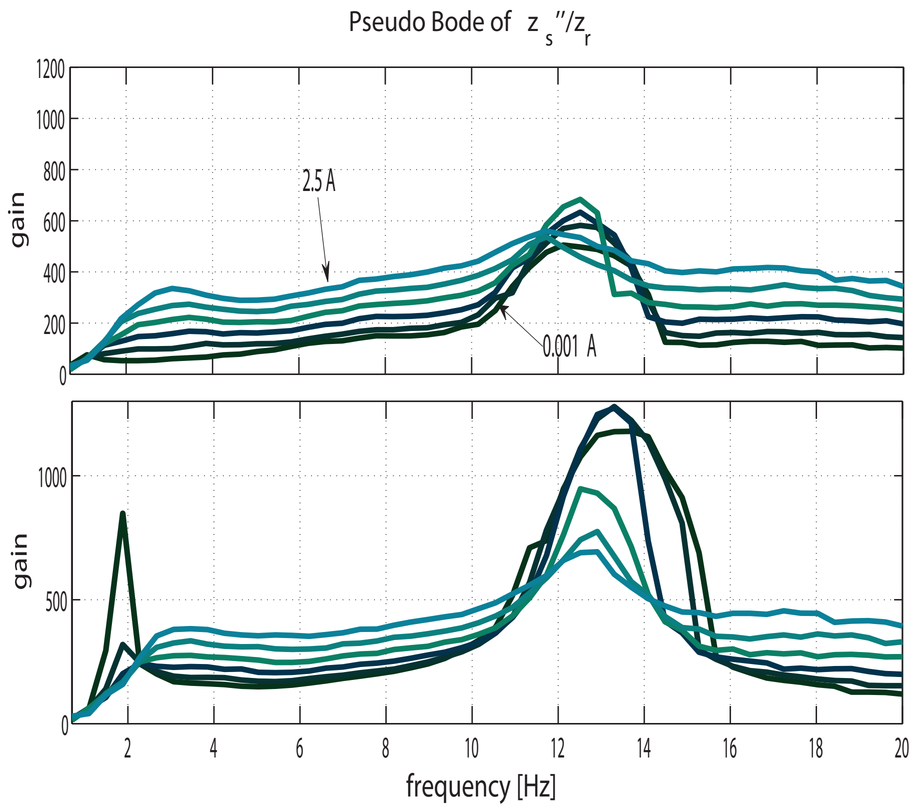

Fig. 6 Performance of semi-active suspensions, with and without hysteresis, in order to modify the control objective (comfort) in a semi-active suspension in the span of 0-2.5 A of current. Top plot is the *linear QoV* case, bottom plot is the *nonlinear QoV* case.

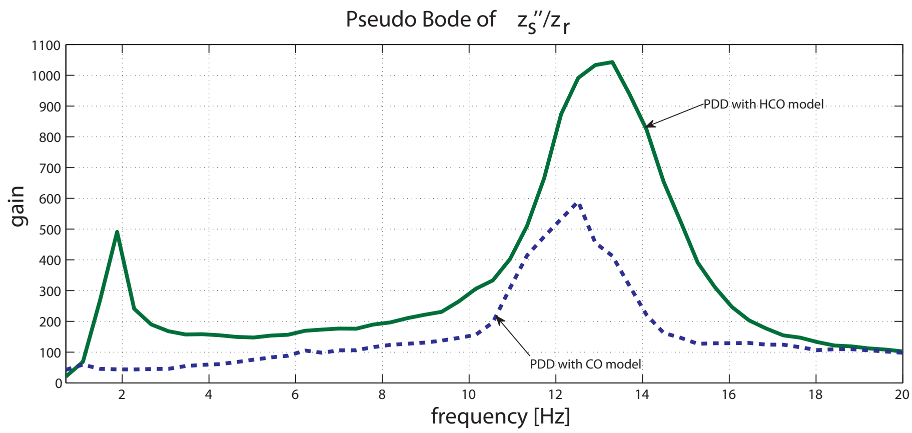

Fig. 7 Performance of the semi-active suspension, with and without hysteresis, in closed loop for the *PDD* controller.

6 Conclusion

This work proposes a *MR* damper model called (HCO) with several features: a simple structure, standard identification procedure, precision in hysteresis simulation, and proper structure for controller synthesis. This modelling approach is compared with a model based on transient response. A study case, a Quarter of Vehicle with a *MR* damper shows that the hysteresis could affect the primary ride and vehicle handling. Missing the hysteresis phenomenon decreases the negative effects on the rattle-space and tire-hop frequencies. Hence, this work focuses the attention to more accurate specification in the simulation of vehicle behavior for controller evaluation purposes. The example was illustrative and requires more analysis.

7 References

[1] S. Duym. An Alternative Force State Map for Shock Absorbers. *IMechE Proc Instn Mech Engrs Part D*, 211:175–179, 1997.

[2] M. Wiegel, W. Mack, and A. Riepl. Nonparametric Shock Absorber Modelling Based on Standard Test Data. *Vehicle Systems Dynamics*, 38:6:415–432, 2002.

[3] A. Simms and D. Crolla. The Influence of Damper Properties on Vehicle Dynamic Behavior. In *Steering and Suspension Technology Symposium SAE 2002 World Congress, Detroit Michigan, March 4-7*, 2002.

[4] J. A. Calvo, B. Lopez-Boada, J. L. San Roman, and A. Gauchia. Influence of a Shock Absorber Model on Vehicle Dynamic Simulation. *Proc. IMechE Part D: J. Automobile Engineering*, 223:189–202, 2009.

[5] L. X. Wang and H. Kamath. Modelling Hysteretic Behavior in MR Fluids and Dampers using Phase-Transition Theory. *Smart Mater. Struct.*, 15:1725–1733, 2006.

[6] R. Stanway, J. L. Sproston, and N. G. Stevens. Non-linear modelling of an electro-rheological mr damper. *Journal of Electrostatics*, 20:167–184, 1987.

[7] B. F. Spencer Jr, S. J. Dyke, M. K. Sain, and J. D. Carlson. Phenomenological Model of a MR Damper. *J. Engrg. Mech.*, 123(3):230–238, 1997.

[8] S. B. Choi, S. K. Lee, and Y. P. Park. A Hysteresis Model for Field-Dependent Damping Force of a Magnetorheological Damper. *Sound and Vibration*, 245:375–383, 2001.

[9] S-B. Choi and K-G. Sung. Vibration Control of Magnetorheological Damper System subjected to Parameter Variations. *Int. J. Vehicle Design*, 46(1):94–110, 2008.

[10] S. Guo, S. Yang, and C. Pan. Dynamical Modeling of Magneto-rheological Damper Behaviors. *Int. Mater, Sys. and Struct.*, 17:3–14, 2006.

[11] A. C. Shivaram and K. V. Gangadharan. Statistical Modeling of a MR Fluid Damper using the Design of Experiments Approach. *Smart Mater. and Struct.*, 16(4):1310–1314, 2007.

[12] J. de-J. Lozoya-Santos, R. Morales-Menendez, and R. A. Ramirez-Mendoza. Magneto-Rheological Damper Modelling. In *Proceedings of the Int. Conf. on Modelling, Simulation and Validation, MSV 09, Worldcomp'09. Las Vegas, Nevada, USA, July 15*, pages 92–98, 2009.

[13] S. M. Savaresi, S. Bittanti, and M. Montiglio. Identification of Semi-Physical and Black-Box Non-Linear Models: the Case of MR-Dampers for Vehicles Control. *Automatica,*, 41(1):113–127, 1 2005.

[14] J-H Koo, F. D. Goncalves, and M. Ahmadian. A Comprehensive Analysis of the Response Time of MR Dampers. *Smart Mater. Struct.*, 15:351–358, 2006.

[15] J. Takács. A phenomenological Mathematical Model of Hysteresis. *COMPEL*, 20:4:1002–1014, 2001.

[16] J. de-J. Lozoya-Santos, R. Morales-Menendez, R. A. Ramirez-Mendoza, and E. Nino-Juarez. Frequency and Current Effects in a *MR* Damper. *International Journal of Vehicle Autonomous Systems*, 7:3:121–140, 2009.

[17] C. Poussot-Vassal, O. Sename, L. Dugard, P. Gáspár, Z. Szabó, and J. Bokor. A New Semi-active Suspension Control Strategy through LPV Technique. *Control Engineering Practice*, 16(12):1519–1534, 2008.

[18] S. M. Savaresi, E. Silani, S. Bittanti, and N. Porciani. On Performance Evaluation Methods and Control Strategies for Semi-Active Suspension Systems. In *Proceedings of the 42nd IEEE Conference on Decision and Control, Maui, Hawaii USA, December*, 2003.

[19] R. Morselli and R. Zanasi. Control of Port Hamiltonian Systems by Dissipative Devices and its Application to improve the Semiactive Suspension Behavior. *Mechatronics*, 18:364–369, 2008.

[20] D. Sammier, O. Sename, and L. Dugard. Skyhook and H_∞ Control of Active Vehicle Suspensions: Some Practical Aspects. *Vehicle Systems Dynamics*, 39(4):279–308, 2003.